AGU PUBLICATIONS

JGR

Journal of Geophysical Research: Atmospheres

RESEARCH ARTICLE

10.1002/2014JD022156

Key Points:
- Quantifying OC aerosol light absorption in snow
- Comparing two techniques for estimating absorption by aerosol type
- Quantifying aerosol light absorption by iron in snow

Correspondence to:
C. Dang,
chengd1@atmos.washington.edu

Citation:
Dang, C., and D. A. Hegg (2014), Quantifying light absorption by organic carbon in Western North American snow by serial chemical extractions, *J. Geophys. Res. Atmos.*, *119*, 10,247–10,261, doi:10.1002/2014JD022156.

Received 9 JUN 2014
Accepted 14 AUG 2014
Accepted article online 18 AUG 2014
Published online 10 SEP 2014

Quantifying light absorption by organic carbon in Western North American snow by serial chemical extractions

Cheng Dang[1] and Dean A. Hegg[1]

[1]Department of Atmospheric Sciences, University of Washington, Seattle, Washington, USA

Abstract Light-absorbing particulates (LAPs) in snow, namely black carbon (BC), organic carbon (OC), and iron oxides, can reduce snow albedo and influence regional and global climate. Partitioning light absorption by LAPs to BC and non-BC (i.e., OC and iron oxides) is important yet difficult due to both technical limitations and the complicated nature of LAPs. In this work, we applied serial chemical extractions on LAP samples acquired from snow samples in western North America to study the light absorption by different types of OC. We also estimated the light absorption due to iron oxides. Based on these chemical analyses, we then compared our estimation of the non-BC light absorption with that from an optical method. The results suggest that humic-like substances (sodium hydroxide (NaOH)-soluble), polar OCs (methanol-soluble), and iron oxides are responsible for 9%, 4%, and 14% (sample means) of the total light absorption, respectively, in our samples, though it should also be noted that there is great variance in these means. The total light absorption due to non-BC LAPs estimated by chemical methods is lower than that estimated by optical method by about 10% in all sampling regions. Reasons for this difference are explored.

1. Introduction

It is now widely accepted that deposition of black carbon (BC) and other light-absorbing particulates (LAPs) on snow and ice surfaces has a significant impact on regional and global climate [*Bond et al.*, 2013; *Intergovernmental Panel on Climate Change*, 2013]. Recent studies have further suggested that non-BC particulates are responsible for a large fraction of the particulate light absorption that reduces the reflectivity of snow and ice cover [*Doherty et al.*, 2010; *Wang et al.*, 2013; *Zhang et al.*, 2013]. The chemical identity of the non-BC absorbers in the deposition aerosol encompasses both iron oxides and a wide variety of organic species, which derive from numerous sources (e.g., soil, biomass burning, and industrial emissions), similar to but by no means congruent with the sources of BC itself [e.g., *Bond et al.*, 2013]. Hence, from the standpoint of quantifying the sources of light-absorbing particulates deposited on snow and ice cover, and the intimately related issue of the formulation of effective mitigation strategies, it is important to know the partitioning of light absorption between BC and the various non-BC aerosol species.

Partitioning of aerosol light extinction based on chemical composition has a long history, but the traditional approach, based on an extinction closure calculation coupled with composition mass closure, is fraught with uncertainties [cf., *White*, 1990]. Essentially, one determines the aerosol composition based on various chemical measurement techniques and then either assigns a mass absorption (or extinction) efficiency to each chemical component a priori or derives one from a multiple linear regression of the total absorption onto the various chemical masses. If the number of chemical species is quite large, the regression coefficients become highly uncertain without additional constraints on the coefficients, i.e., essentially a priori assumptions though in some cases based on limited laboratory data. Perhaps the most widely known of such approaches is that used in the IMPROVE study [*Pitchford et al.*, 2007]. The regression-derived coefficients (absorption efficiencies) for various chemical classes based on that very large database have been widely used in subsequent work [e.g., *Kim et al.*, 2013; *Yang et al.*, 2012]. Nevertheless, the application of such quasi-empirical parameterizations to data sets other than those upon which they are based has always been somewhat problematic.

Another more recent approach to partitioning the aerosol absorption between BC and non-BC components, and one which moreover has been extensively applied to aerosols deposited on snow and ice surfaces, is a physical/optical approach in which the wavelength dependence of the measured light absorption is

©2014. American Geophysical Union. All Rights Reserved.

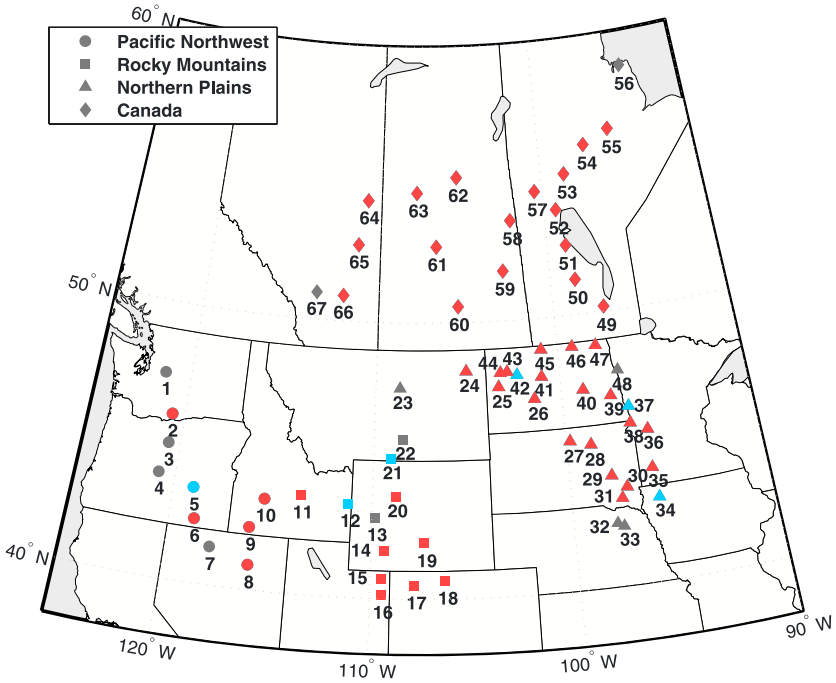

Figure 1. Snow sampling locations with sites numbered chronologically. Red: inductively coupled plasma mass spectrometry (ICP-MS) and chemical extraction data available. Blue: chemical extraction data available. Grey: no chemical data available.

used to differentiate BC from non-BC absorption. Essentially, this approach takes advantage of the lack of wavelength dependence of light absorption (quantified by the absorption Ångström exponent, here denoted Å) by BC relative to virtually anything else occurring in the natural environment. The method was first applied to snow by *Clark and Noone* [1985]. The details of this methodology are given by *Grenfell et al.* [2011], and examples of its application to large data sets have been given by *Doherty et al.* [2010] and *Wang et al.* [2013]. The ease of application of this method renders it very attractive, but it is not deterministic and involves an a priori assumption of Å of the non-BC aerosol. This can lead to large uncertainties in the partitioning estimates [see *Doherty et al.*, 2010, Figure 16]. Furthermore, the method cannot resolve, by itself, absorption due to the various potential classes of non-BC light absorbers such as iron oxides and various organic species.

In this study, we employ a novel approach to partitioning the light absorption of particles deposited on snow, namely, the serial chemical extraction of particles filtered from melted snow samples, where the absorption of the residual particles after each extraction solvent is measured directly with a modified version of the spectrophotometer of *Grenfell et al.* [2011]. Results from this technique are then compared with the physical/optical technique and an assessment made of possible biases in both approaches.

It is worth noting that there are also soluble organic impurities in snow, which would pass through our filters. How much sunlight might they absorb? Soluble impurities in snow ("chromophores") were studied by *Beine et al.* [2011] at Barrow, Alaska. The soluble impurities absorb significantly at ultraviolet wavelengths (200–300 nm) but much less at the longer wavelengths where solar energy peaks. Figure 1 of Beine et al. shows the absorption coefficient (on base-10) versus wavelength for a typical sample of meltwater. Converting to base-e for comparison, the absorption by soluble impurities at 400 nm is equivalent to that of 0.14 ng/g BC; at the mid-visible wavelength of 550 nm the absorption is equivalent to 0.07 ng/g BC. The BC mixing ratio at Barrow before onset of melt is 10–30 ng/g [*Doherty et al.*, 2013], similar to the values found at the 67 sites studied in this paper, and particulate non-BC is responsible for comparable absorption. While this analysis does not categorically preclude a significant role for absorption by soluble organics at our sample sites, we feel that large enhancements in the relatively rare organics that absorb at visible wavelengths are unlikely for our sites and treat them no further in this paper. The acronyms and symbols used in this paper are listed in Table 1.

©2014. American Geophysical Union. All Rights Reserved.

Table 1. Acronyms and Symbols

Acronyms	
LAP	Light-absorbing particulates
BC	Black carbon
OC	Organic carbon
nonBC	Non-black carbon light-absorbing particulates
ICP-MS	Inductively coupled plasma mass spectrometry
PAOD	Particulate light absorption optical depth
tot	Appears as subscript. Denoting all LAP of LAP samples.
MAC	Mass absorption coefficient
DCM	Dichloromethane
Symbols	
$Å_j$	Absorption Ångström exponent of constituents j
$\tau^i_{abs,j}(\lambda)$	PAOD of constituents j (after chemical extraction stage i) at wavelength λ
$s\tau^i_{abs,j}$	Spectrally integrated $\tau^i_{abs,j}(\lambda)$ across 470 to 700 nm
R^i_j	Fraction of the remaining $s\tau^i_{abs,j}$ (after chemical extraction stage i)
r_{nonBC}	The fraction of PAOD due to non-BC absorbers at 525 nm
f_j	The fraction of PAOD due to constituents j across 470 to 700 nm
I	Transmitted light intensity

2. Methods

2.1. Samples

From January to March 2013, snow samples were collected at 67 sites in western North America, ranging from Nevada to Manitoba. These sites are numbered chronologically and are distributed as shown in Figure 1. At all sites, samples were collected for photometric analysis of LAPs (Light Absorbing Particles) on nuclepore filters. Additionally, at 56 of the 67 sites, a snow pit was dug, and three adjacent depth profiles were obtained (i.e., samples of snow at various snow depths were obtained). The depth profiles were all within 1 m of each other, and the sample depths were uniform across the profiles. For the exterior left and right profiles plastic bags and pre-cleaned glass jars were, respectively, used to store the samples, which were later melted and filtered through nuclepore filters for analysis by the (ISSW) Integrating Sandwich and Integrating Sphere (rationalization of the container selection is given below). For the central profile, at 56 of the 67 sites, samples were stored in pre-cleaned glass jars and later melted and filtered through GHP filters (GH Polypro filter, hydrophilic polypropylene, Pall Life Sciences, www.pall.com). The GHP filters were utilized in the serial chemical extraction procedure. For each of the GHP filters, a fraction of the meltwater before filtration was saved in pre-cleaned glass jars and kept frozen until analyzed in the laboratory for chemical composition. Hence, for each of the sites for which GHP samples were obtained, we have the GHP filter itself, two nuclepore filters from closely adjacent, bracketing locations and the same snow depth, one derived from snow stored in a plastic bag and one from snow stored in glass, and an unfiltered snow sample for chemical analysis. A more detailed snow sampling procedure can be found in (Doherty et al, Black carbon and other light-absorbing particles in snow of central North America, submitted to Journal of Geophysical Research., 2014). In this paper, we will call the LAPs collected by GHP filters and nuclepore filters the GHP LAP samples and nuclepore LAP samples, respectively. The rationalization for this rather elaborate suite of samples is as follows.

In our previous large-area surveys of BC in snow [*Doherty et al*., 2010; *Wang et al*., 2013], nuclepore filters and plastic bags were used because the former are ideal for optical measurement and the latter are easy to carry in the field. However, for chemical analysis, nuclepore filters are too fragile, and past work has suggested that some plastic bags can lead to artifacts in LAP measurements [e.g., *Wang et al*., 2013]. Therefore, for the chemical analysis in this paper, we used only the samples collected in glass jars and chemically robust GHP filters. The glass jars used for both collecting snow and saving snowmelt are manufactured by I-CHEM, pre-cleaned by them to US-EPA (United State Environmental Protection Agency) level II specifications, and available through VWR (www.vwr.com).

Although GHP LAP samples are optimized for chemical analysis, they are not ideal for optical analysis. In the comparison of optical results between GHP LAP samples and nuclepore LAP samples, the absorption optical depth and absorption Ångström exponent of GHP LAP samples are biased low by 50% (not shown in this paper), likely induced by the difference in filter matrices. However, to evaluate the results of chemical analysis with respect to light absorption, good, consistent absorption optical depths as a function of wavelength are needed. These optical depths were obtained from an average of the two nuclepore LAP samples that were co-collected with the GHP LAP samples. (Note that, for the plastic bags we utilized in this study, differences between the LAP concentrations derived from the bag samples and those from the glass jars proved insignificant.) This procedure has the advantage of leading to optical depth (and thus LAP estimates) that is completely comparable with our previous extensive measurements. It should also be noted

©2014. American Geophysical Union. All Rights Reserved.

that breakthrough tests indicate that the GHP and nuclepore filters have similar retention efficiencies for particles, essentially complete retention down to 0.2 μm diameter.

In this paper, we used 100 GHP LAP samples, 58 snow water samples, and 100 pairs of nuclepore LAP samples. The GHP LAP samples, as mentioned above, were used for serial chemical extraction and were measured in the spectrophotometer to quantify changes in particulate light absorption as various types of organic carbon (OC) were removed from the filters. The snow water samples were analyzed by inductively coupled plasma mass spectrometry (ICP-MS) to estimate the concentration of iron, from which we estimate light absorption by iron oxides. Iron oxides are a significant light-absorbing component in most soils, particularly those rich in mineral dust. The nuclepore LAP samples were measured in the spectrophotometer to calculate absorption Ångström exponent (a variable that describes the wavelength dependence of absorption; the mathematical definition can be found in section 2.2) of all LAPs and to make an estimate of the partitioning of light absorption to BC and non-BC components from the optical data alone.

2.2. Optical Analysis of Nuclepore LAP Samples

The LAP samples were measured with a modified ISSW spectrophotometer to quantify the light absorption due to LAPs in snow and to partition the light absorption due to BC and non-BC LAPs. A description of an earlier version of the ISSW spectrophotometer was given by *Grenfell et al.* [2011]. The modified version of the ISSW has replaced the integrating sandwich above the sample filter with a second integrating sphere. Both versions of ISSW spectrophotometers are designed to be sensitive to light absorption but not scattering and are thus appropriate for quantifying the light absorption due to LAPs in snow. A brief introduction of the optical analysis is given in this section; a more detailed presentation can be found in paper *Grenfell et al.* [2011].

The ISSW spectrophotometer measures the light attenuation spectrum from 400 to 700 nm due to all LAPs collected on a filter. The spectrum of light attenuation is then calibrated against a set of fullerene (Alfa Aesar, Inc., Ward Hill, MA USA) standard samples to determine the equivalent loading of a LAP sample. This equivalent loading quantifies the mass of fullerene needed to produce the same amount of light attenuation, within a given wavelength range, as that of the corresponding LAP sample. Because the ISSW spectrophotometer is nominally sensitive to light absorption but not scattering, spectral equivalent loading is converted into spectral absorption optical depth by multiplying the spectral mass absorption coefficient of fullerene, which is estimated to be ~ 7.2 m^2/g at 550 nm. These values are estimated based on the comparison between fullerene and another synthetic BC (Monarch-71) that has a known mass absorption coefficient [*Clarke et al.*, 1987]. For clarity and simplicity, here we will use particulate light absorption optical depth (PAOD) to denote the total particulate absorption optical depth of the particles on the filter.

The ISSW spectrophotometer responds to all constituents on the filter. Therefore, the derived loading is the result of light absorption by all constituents. To separate the absorption contribution from BC versus non-BC LAPs (i.e., OC and iron oxides), we make use of differences in their wavelength dependence of absorption following *Grenfell et al.* [2011]. For BC, the light absorption varies only slightly over the visible band, but, for non-BC, the absorption increases toward the blue and the UV band. This dependence of absorption on wavelength is described by the absorption Ångström exponent $Å = -\frac{\ln[\tau_{abs}(\lambda_1)/\tau_{abs}(\lambda_2)]}{\ln(\lambda_1/\lambda_2)}$: where τ_{abs} is the absorption optical depth at wavelength λ. Here, Å is quantified for $\lambda_1 = 450$ nm and $\lambda_2 = 600$ nm, because this is the wavelength range over which absorption Ångstrom exponent of BC and non-BC LAPs has most commonly been measured and the measured values are needed for the optical analysis. The calculated Å is Å at 525 nm, which is the mid-point of 450–600 nm. Å of all LAP on a filter from our snow samples, $Å_{tot}$, is due to a mix of BC and non-BC absorbers and so will be intermediate between $Å_{BC}$ and $Å_{nonBC}$ (with appropriate assumptions). We therefore use $Å_{tot}$ to apportion the light absorption due to BC and non-BC constituents, if $Å_{BC}$ and $Å_{nonBC}$ are known [*Grenfell et al.*, 2011; *Doherty et al.*, 2010]. In this study, we assume $Å_{BC} = 1.1$. This is consistent with previous studies that have measured $Å_{BC}$ for atmospheric aerosol [e.g., *Bond*, 2001]. The value of $Å_{nonBC}$ varies from sample to sample depending on the mix of non-BC absorbers present. These were estimated based on measured values of Å for site-specific soil samples taken concurrently with the snow samples and similarly analyzed, along with an estimate of Å for combustion aerosol OC taken from *Doherty et al.* [2010] (i.e., $Å_{combustion\ OC} = 5$). The relative contributions of soil and combustion OC to $Å_{nonBC}$ were estimated by receptor modeling of the LAP sources [*Hegg et al.*, 2010]. These relative contributions are then used to weight the Å

©2014. American Geophysical Union. All Rights Reserved.

of soil samples and combustion OC to calculate the $Å_{nonBC}$. In comparison to the value of $Å_{combustion\ OC} = 5$, measured values of Å for site-specific soil samples ranged from 2.31 to 6.55 with a mean of 3.89 and a standard deviation of 0.84. We note that the ratio of the average contribution of soil versus combustion OC to absorption, based on the PMF model, is 2.1 and individual sample ratios varied between 0.05 and 47.

In this paper, we will use the following three metrics for the LAP samples:

1. $\tau_{abs,tot}(\lambda)$: the PAOD of all LAPs deposited on the filter across 400–700 nm.
2. $Å_{tot}$: the absorption Ångström exponent of all LAPs deposited on the filter, measured 450 to 600 nm.
3. f_{nonBC}: the fraction of PAOD caused by non-BC absorbers across 470–700 nm. This metric is calculated using the following equation:

$$f_{nonBC} = \frac{\int_{470}^{700} \tau_{abs,nonBC}(\lambda)\, d\lambda}{\int_{470}^{700} \tau_{abs,LAP}(\lambda) d\lambda} \tag{1}$$

where $\tau_{abs,nonBC}$ is the PAOD due to non-BC absorbers. This is estimated using assumed values of $Å_{BC}$ and $Å_{nonBC}$ as described below. (Note that this is distinct from the parameter f^{est}_{nonBC} of *Doherty et al*. [2013] and *Wang et al*. [2013], in that the latter is calculated by weighting absorption optical depth by the downwelling solar irradiance and then integrating across 300–750 nm.)

Based on equation (10) of *Grenfell et al*. [2011], the fraction of PAOD due to non-BC at 525 nm is given by:

$$r_{NBC} = \frac{\tau_{NBC}(525nm)}{\tau_{tot}(525nm)} = \frac{Å_{tot} - Å_{BC}}{Å_{NBC} - Å_{BC}} \tag{2}$$

From this we can estimate the PAOD of BC ($\tau_{abs,BC}$) and non-BC ($\tau_{abs,nonBC}$) at 525 nm based on the measured PAOD due to all LAPs ($\tau_{abs,tot}$) at 525 nm. The $\tau_{abs,BC}$ at 525 nm is then extrapolated to 470–700 nm using $Å_{BC} = 1.1$, to calculate spectrally resolved $\tau_{abs,BC}$. Spectrally resolved $\tau_{abs,nonBC}$ is then given by $\tau_{abs,tot}$ minus $\tau_{abs,BC}$ at each wavelength.

To evaluate f_{nonBC}, it is important to note that $Å_{nonBC}$ is different for different types of non-BC LAPs and may vary from 2 to > 10 [*Doherty et al*., 2010 and references therein]. In addition, $Å_{BC}$ could theoretically be as low as 0.8 or as high as 1.6 [*Lack and Cappa*, 2010]. Therefore, if $Å_{nonBC}$ of the non-BC absorbers deposited on a filter differ from the assumed value, or if $Å_{BC}$ is significantly different from 1.1, the estimated fractional absorption from non-BC will be biased high or low, possibly by up to a factor of 2 [*Doherty et al*., 2010, Figure 16]. We explore this issue with sensitivity studies in section 3.2.

2.3. ICP-MS Analysis for Iron

The main light-absorbing iron oxides are in the form of hematite or goethite [*Lafon et al*., 2004, 2006], and these oxides are found in most soils. To quantify the light absorption due to iron oxides, we first measured the iron concentration in acidified snow water samples using ICP-MS [*Lafon et al*., 2004; *Wang et al*., 2013]. Then, assuming all the iron came from either goethite or hematite, we derived the concentration of iron oxides in snow samples. These concentrations are converted into the PAOD of iron oxides by assuming the mass absorption coefficient (MAC) of the Fe is 0.8 m^2/g [*Alfaro et al*., 2004] at 550 nm. This PAOD at 550 nm is then extrapolated to the wavelength range from 400 to 700 nm assuming $Å_{Fe} = 3$ [*Alfaro et al*., 2004]. Assuming that all the iron oxides in the snowmelt were captured by the filters, the fractional absorption optical depth due to iron oxides (f_{Fe}) can be calculated based on equation (1), but with $\tau_{abs,Fe}$ in place of $\tau_{abs,nonBC}$.

2.4. Serial Chemical Extraction on GHP LAP Samples

The chemical composition and sources of OC are variable and complex. As discussed in the introduction, this can lead to large uncertainties in estimating light absorption employing traditional extinction budget approaches. We avoid this by measuring directly the absorption of several different classes of OC found on our sample filters.

Inspired by previous research [*Havers et al*., 1998; *Kirchstetter et al*., 2004; *Polidori et al*., 2008; *Chen and Bond*, 2010], we use chemical solvents to extract different types of OC from the GHP samples. In this research, four

©2014. American Geophysical Union. All Rights Reserved.

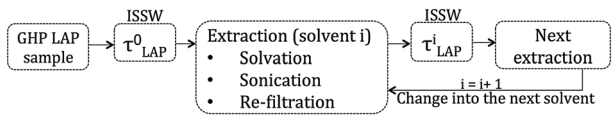

Figure 2. Flow chart illustrating the procedure of the chemical extraction experiment.

chemical solvents were selected. Three of them are organic chemical solvents: methanol, dichloromethane (DCM), and hexane. These solvents are listed in the order of decreasing polarity and can be used sequentially to dissolve both polar and non-polar OC. The fourth solvent is inorganic: sodium hydroxide (NaOH), which reacts with sparingly soluble humic-like substances (HULIS), so that they can be extracted in water solution.

As shown in Figure 2, before any chemical extraction, all GHP LAP samples were first measured with the ISSW spectrophotometer [*Grenfell et al.*, 2011] to calculate the PAOD by all LAPs in the snow ($\tau^0_{abs,tot}(\lambda)$). The GHP LAP samples were then extracted with methanol, DCM, hexane, and NaOH successively, and the filters re-measured in the ISSW after each extraction step. This way we could measure the decrease in $\tau_{abs,tot}$ with each extraction step.

In this extraction process, for each selected solvent, GHP LAP samples were put in individual glass jars and soaked in 40 ml of chemical solvent, then sonicated with the solvent for 15 min and allowed to sit for 18 to 20 h. The solution was then drawn through the extracted GHP filter to recapture the particles that were not dissolved in the solvent but became suspended in the solution during soaking or sonicating. During re-filtration, filters and jars were carefully cleaned with the extraction chemical, to prevent the loss of LAPs to the back and edge of the filter and to the glass wall of the container. Tests run with fullerene standards suggested no significant loss of mass during the extraction process.

In preliminary chemical extraction tests on 8 GHP LAP samples, the amount of OC that dissolved in hexane was large. Therefore, the volume of hexane was doubled to 80 ml per sample to prevent saturation. Moreover, hexane appears to swell the irregular and fiber-like polypropylene material that comprises the filter pores, thus constricting the pores and reducing the flow of filtrate. The swelling diminishes and the flow rate recovers after the filters dry out. Considering this problem, each GHP LAP sample was soaked in hexane for 4 to 5 h and then dried overnight before re-filtration.

Coupled with chemical extraction, the GHP LAP samples were measured in the ISSW spectrophotometer both before and after each chemical extraction ($\tau^i_{abs,tot}(\lambda)$), to evaluate the change in PAOD of LAP samples. The light absorption due to OC increases at shorter wavelengths (i.e., $Å_{OC} > 0$), so the metric used to test for a change in absorption is the spectrally integrated $\tau_{LAP}(\lambda)$ over a broad mid-visible wavelength range. The ISSW data have poor signal to noise for $\lambda < 420$ nm and $\lambda > 700$ nm due to a weak light signal. Based on the tests of how chemical extractions affect the GHP filters (section 2.5.1), we determined that the optical properties of the GHP filters cannot be reliably determined for $\lambda < 470$ nm. Therefore, at each extraction step, the light absorption by LAP on the GHP filters is characterized by the spectrally integrated PAOD from 470 nm to 700 nm. The procedure for estimating the apportionment of light absorption between the various solvent extracts is as follows.

We denote $s\tau^i_{abs,tot}$ as the spectrally integrated PAOD of GHP LAP samples, where the superscript i denotes the extraction stage, ranging from un-extracted (i.e., i = 0) to NaOH-extracted (i = NaOH) filter. The value of $s\tau^i_{abs,tot}$ at the ith stage of extraction is:

$$s\tau^i_{abs,tot} \equiv \int_{470}^{700} \tau^i_{abs,tot}(\lambda)d\lambda \tag{3}$$

Compared with the PAOD of the untreated GHP LAP sample (i = 0), the ratios of the remaining $s\tau^i_{abs,tot}$ after chemical extraction are:

$$R^i_{tot} = \frac{s\tau^i_{abs,tot}}{s\tau^0_{abs,tot}} \tag{4}$$

Because the NaOH extraction is the final step of the chemical extractions, the PAOD reduced after this stage is the PAOD due to all extractable OC in the LAP samples. In order to compare the chemical method with

©2014. American Geophysical Union. All Rights Reserved.

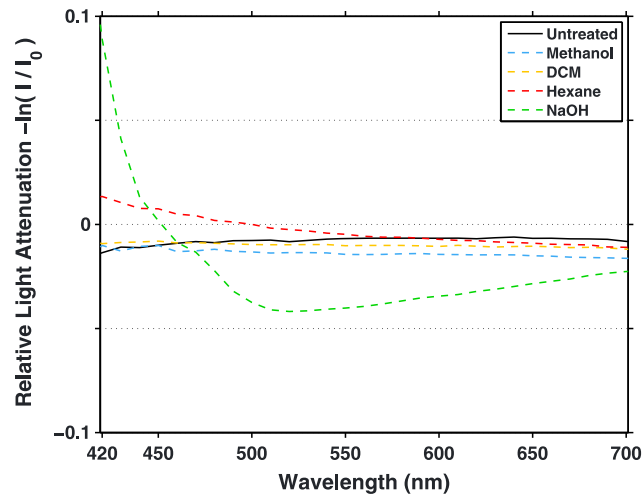

Figure 3. Effect of chemical solvents on spectrum of relative light attenuation for blank GHP filters. Each curve is an average of five blank GHP filters. The black curve shows the value for untreated blanks; blue, yellow, red, and green show the value for blanks after successive extractions using methanol, dichloromethane (DCM), hexane, and sodium hydroxide (NaOH), respectively.

the optical analysis discussed in section 2.2, we calculate the fraction of PAOD due to chemically extractable OC (f_{OC}) in a way analogous to the optically derived non-BC fraction of absorption (f_{nonBC}; equation (1)):

$$f_{OC} = \frac{\int_{470}^{700} \tau_{abs,tot}^{0}(\lambda)\, d\lambda - \int_{470}^{700} \tau_{abs,tot}^{NaOH}(\lambda)\, d\lambda}{\int_{470}^{700} \tau_{abs,tot}^{0}(\lambda) d\lambda} \tag{5}$$

Equation (5) assumes that the measured change in PAOD after all chemical extractions is due only to the change in the amount of organics on the filters. However, the relative light attenuation of a given LAP sample as measured with the ISSW is in reference to a blank GHP filter that has not been treated with any chemical solvent. If the optical properties of the GHP filter used to capture LAPs are themselves altered by exposure to the extraction chemicals, or if the chemical causes a change in the interaction between LAPs and the GHP filter, the relative light attenuation will change even if no LAP is extracted from the filter. To examine the influence of chemical extractions on the GHP filter and on the interaction between the GHP filter and LAPs, the following tests were done.

2.5. Tests on GHP Blank Filters and GHP Fullerene Samples

2.5.1. Test on Blank GHP Filters

To test the effect of the extraction chemicals on the optical properties of the GHP filter itself, serial extractions were applied to five blank GHP filters following the same procedure that was used on the field filters. Their averaged relative light attenuation from 420 to 700 nm is shown in Figure 3. Each of these five blank GHP filters (i.e., transmitted intensity I) was compared against a GHP blank that had not been exposed to the extraction chemicals (i.e., transmitted intensity I_0) and which served as a reference GHP filter through the whole test. Therefore, if the relative light attenuation ($-\ln(I/I_0)$) is zero, it means that the GHP blank exposed to extraction chemicals produces the same light attenuation as the unexposed reference, i.e., that the light-absorbing properties of the filters are unaltered by the extraction chemicals.

As Figure 3 shows, the relative light attenuation of the untreated GHP blanks (black line in Figure 2.3) is slightly lower than zero, ~ 0.01; this is because the optical properties of blank un-extracted GHP filters are not entirely identical to each other. Testing on 11 new GHP blank filters indicates that the transmitted light signal through individual GHP filters differs from the mean by 0.2%–1%. After exposure to methanol and DCM analogous to that during extraction, the spectral relative light attenuation changed by < 0.005 at all wavelength compared with the reference GHP blank. This apparent change is on the same order as

©2014. American Geophysical Union. All Rights Reserved.

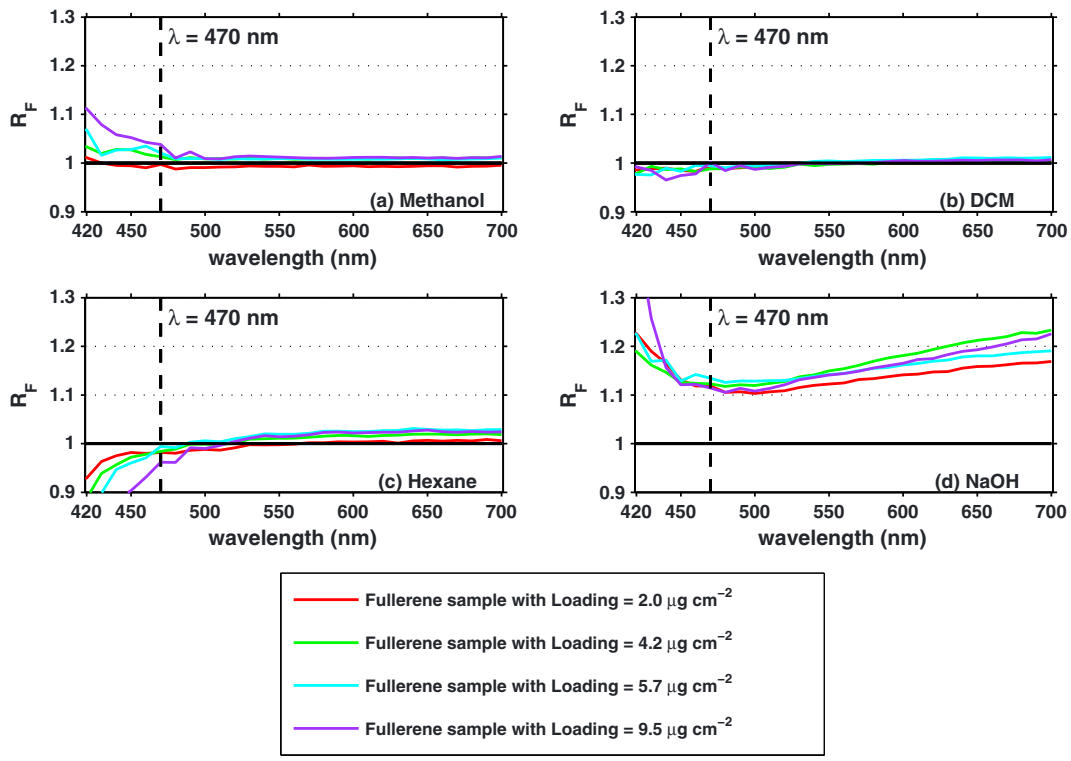

Figure 4. Ratio R_F^i of GHP fullerene samples after each extraction stage i: methanol, DCM, hexane, and NaOH.

the variation in signal between multiple unaltered blanks and so is insignificant. After exposure to hexane, $-\ln(I/I_0)$ for the GHP filter increased steadily with wavelength from 700 to 420 nm, but the change is still < 0.01 even at the shortest wavelengths. After exposure to NaOH, $-\ln(I/I_0)$ decreased gradually from 700 to 500 nm, then increased toward shorter wavelengths to ~ 0.1, which is a significant change. As there were no LAPs on these filters, these changes of $-\ln(I/I_0)$ must have been caused by a change of the optical properties of the GHP filter itself, caused by soaking in the chemicals.

2.5.2. Test on GHP Fullerene Samples

To investigate the influence of chemical solvents on the interaction between LAPs and GHP filters, the same serial extractions were applied to four GHP filters loaded only with fullerene. These fullerene samples were made by drawing different amounts of fullerene suspensions through GHP filters to simulate the deposition of snow LAPs on GHP filters. The amount of fullerene loaded on these filters ranges from 2 to 10 μg/cm^2 to cover the range of loadings on our field GHP LAP samples. As with the blank filters, the fullerene samples were measured in the ISSW spectrophotometer both before and after each chemical extraction. Because fullerene is nominally 100% synthetic BC it should be insoluble in all four extraction chemicals (methanol, DCM, hexane, and NaOH), so the observed change of optical properties with extraction should not be due to a change in the amount of fullerene but instead due to the combined effect of changes in the GHP filters and a change in the interaction between fullerene and the GHP filter resulting from a change in the GHP filter matrix.

The change of absorption for the fullerene-loaded filters can be evaluated by looking at the ratio of spectrally integrated PAOD of fullerene after chemical extraction relative to that before extraction using equation (4) but now with R_F^i. As is shown in Figure 4, after methanol, DCM, and hexane extraction, the ratios vary only slightly around 1.0 from 470 to 700 nm, but increase or decrease by up to 10% at shorter wavelengths (420–470 nm). However, after NaOH extraction, the ratio increased to as high as 1.2 at 700 nm, then decreased gradually to ~1.1 at 470 nm, and then increased rapidly toward 400 nm. This implies that (1) mechanisms that change the apparent PAOD of fullerene samples have stronger impact for the 420 to 470 nm wavelength interval than at longer wavelengths and (2) the NaOH extraction changes the optical properties of the fullerene-loaded filter more than the other chemical extractions. Since all four extractions

©2014. American Geophysical Union. All Rights Reserved.

appear to significantly affect the fullerene-loaded filters at wavelengths shorter than 470 nm, for the extraction analysis we use only PAOD data from 470 to 700 nm.

Based on the results shown in Figure 4, we calculated the dependence of R_F^i on fullerene sample loadings at 10 nm intervals from 470 to 700 nm for each of the four loadings shown in Figure 4. No dependence on loading was observed (not shown in this paper). Therefore, we use the averaged R_F^i of all four fullerene samples (denoted as $R_{F,avg}^i$) at each wavelength to represent the R_F^i at that wavelength. Similar to what was shown in Figure 4, $R_{F,avg}^i$ is near 1.0 after methanol, DCM and hexane extractions, and varies slightly with wavelength. After NaOH extraction, $R_{F,avg}^{NaOH}$ is 1.12 at 470 nm and increases toward 700 nm to 1.20.

These results imply that the chemical extraction of GHP LAP samples may lead to a bias in measured absorption merely due to the extraction, sonication, re-filtration processes, and the related change of GHP filter itself. To correct for this bias, we applied a correction factor to the measured absorption of particles on our GHP LAP samples and then calculated the ratio R_{tot}^i. Specifically, (1) for methanol and hexane extractions, $R_{F,avg}^i$ shows no apparent wavelength dependence with spectrally average value of 1.01, so we multiplied the measured $s\tau_{abs,tot}^i$ of LAP GHP samples by a factor 1.01, then calculated the ratio R_{tot}^i using the measured $s\tau_{tot}^i$ after these two chemical extractions. (2) For hexane extraction, spectrally averaged $R_{F,avg}^{Hexane}$ is 1, so no correction was made for results at this stage. (3) For the NaOH extraction, $R_{F,avg}^{NaOH}$ is wavelength dependent. Therefore, we scaled $\tau_{abs,tot}^0(\lambda)$ of LAP GHP samples by multiplying by the $R_{F,avg}^{NaOH}$ at the corresponding wavelength, then calculated $s\tau_{tot}^0$, and used this scaled $s\tau_{tot}^0$ and measured $s\tau_{tot}^{NaOH}$ to calculate the ratio R_{tot}^{NaOH}.

3. Results

3.1. Chemical Extraction

Figure 5 shows the frequency distribution of the ratio of remaining PAOD of 100 GHP LAP samples after each chemical extraction (R_{tot}^i; equation (4)). The total PAOD of about 50 samples decreased after methanol extraction, while that of fewer than 20 samples increased; for more than 30 samples, $R_{tot}^{Methanol}$ falls within bin 1 ± 0.025, which is also the peak of the frequency distribution. When these samples are then extracted with DCM and the peak of the histogram is still $R_{tot}^{NaOH} = 1 \pm 0.025$. However, compared to the post-methanol extraction, the distribution is wider, leading to both lower and higher values. After hexane extraction, the PAOD decreases further for most of the samples, and the ratio R_{tot}^{Hexane} has a still greater spread. In the final stage, NaOH extraction further reduced the PAOD of most samples; the number of filters in each bin is similar, with no more than 11 in any one bin, and with no obvious mode. Overall, at each extraction stage, the histograms became broader, and they shifted significantly toward the left (lower R_{tot}) after NaOH extraction.

It is clear from the histograms of Figure 5 that the extraction process has substantial uncertainties associated with it, as the ratio R_{tot} of a substantial number of samples exceed unity after each extraction. This is likely due to several reasons. First is the effect of changes in the GHP filter matrix itself during chemical extraction, as discussed in section 2.4, and the resulting uncertainty or noise added to the measurement. Second, it is noteworthy that the exposed area of each filter (circle of 19 mm diameter) is substantially larger than the illumination beam of the ISSW spectrophotometer (circle of about 10 mm diameter). Hence, if the distribution of LAPs on the exposed area of the filters is uneven, a slight change in placement of the filters in the photometer can alter the signal. The precision of the spectrally integrated PAODs based on replicate measurements of untreated GHP samples indicates that variations of $+/-3.5\%$ in R_{tot} on an individual sample could simply be due to this source of uncertainty. Third, other processes leading to artifact signals in R_{tot} are also possible. For example, (1) in the chemical extraction experiment, sonication may change the size distribution of LAPs, and the re-filtration may change the original spatial distribution of LAPs on a filter, and (2) removal of OC and breaking up of large BC particles may lead to a thinner or thicker OC coating on BC, hence a reduced or amplified lensing effect and absorption per mass of BC [*Lack and Cappa*, 2010]. These effects may indeed have contributed to the artifacts revealed in section 2.5.2, and they add uncertainty to the comparison in optical depth between untreated GHP samples and extracted GHP samples.

©2014. American Geophysical Union. All Rights Reserved.

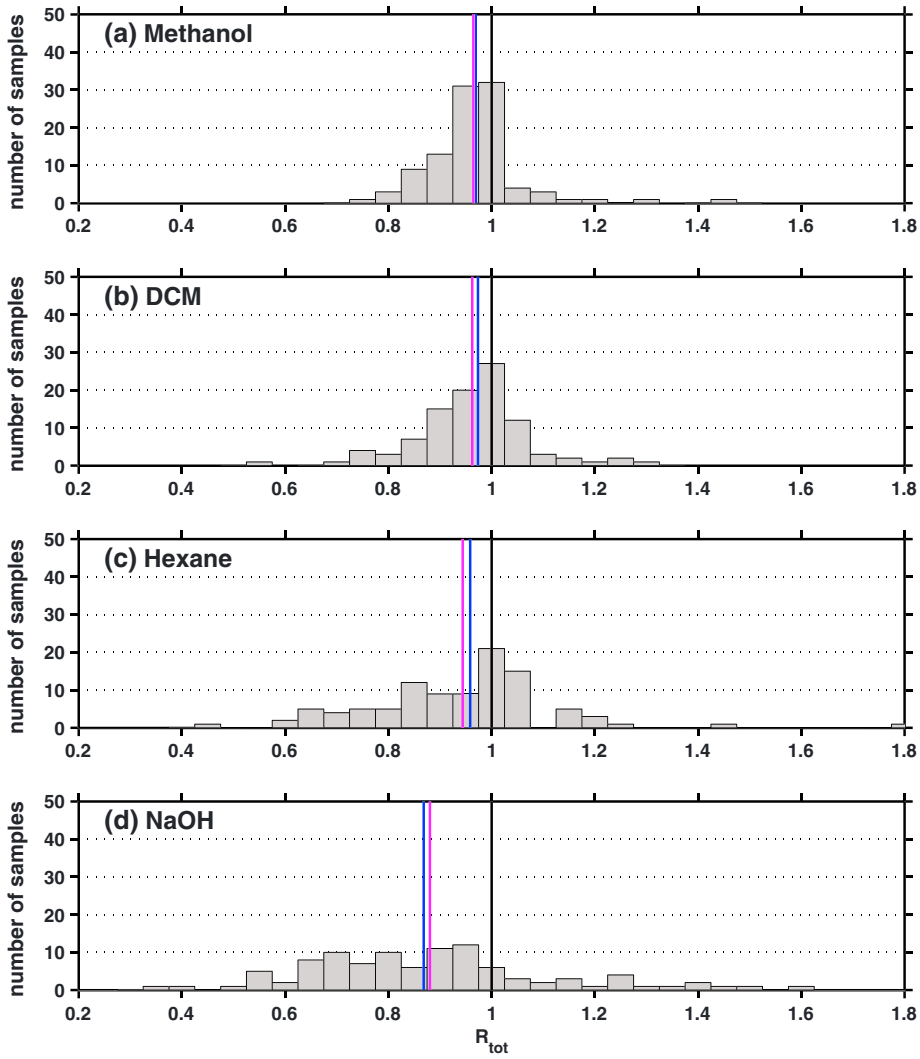

Figure 5. Histograms of the ratio R^i_{tot} of GHP LAP samples after each chemical extraction stage. Data are binned into intervals of $\Delta R_{tot} = 0.05$. The vertical black line shows $R_{tot} = 1$; the pink and blue lines show the median and mean values of R_{tot}, respectively.

As discussed in section 2.5.2, corrections to R_{tot} have been made for GHP samples, but these corrections only partially rectify the influence of chemical extractions on field samples. Changes in the size and spatial distribution of LAPs can occur to different degrees on any filter, and the effects of this on R_{tot} could not be quantified in this experiment on a sample-by-sample basis. Hence, uncertainties preclude a useful comparison in how optical depth changes with extraction for individual samples. However, as demonstrated by the fact that the distributions of R_{tot} get wider with each extraction (Figure 5), the above processes may lead to both positive and negative artifacts. Therefore, while R_{tot} is not robust for any single sample, the distribution of R_{tot} for the entire sample population could still show a significant change after each extraction stage. This suggests that a statistical approach to the extraction data is the proper approach for the analysis. Therefore, we can either examine the changes in optical depth with each extraction stage for the entire sample set, or for subsets of the data that are sufficiently large to reduce the uncertainty in the subset mean to acceptable levels. To this end, population central values and dispersion for each extraction stage are shown in Table 2 with mean and median values denoted in Figure 6.

Because the serial chemical extractions were applied to all GHP samples successively, then compared with the PAOD of untreated samples, the change of total PAOD at each step is a result of the current chemical

©2014. American Geophysical Union. All Rights Reserved.

Table 2. Statistics for the Ratio (R_{tot}) of the Change in Total Absorption Optical Depth of 100 GHP LAP Samples With Each Chemical Extraction Stage

Extraction	Median	Mean	Standard Error	Standard Dev.
Methanol	0.97	0.96	0.01	0.01
DCM	0.96	0.97	0.01	0.11
Hexane	0.94	0.96	0.02	0.22
NaOH	0.88	0.87	0.02	0.24

extraction as well as the extraction in all previous stages. As Figure 5 shows, there are outliers in the R_{tot} ratios at each extraction stage, but the medians and means are close. Therefore, regardless of the outliers, we use mean values to evaluate changes in the ratio R_{tot} and whether the chemical extraction produces any significant changes. After methanol extraction, the PAOD of samples decreased on average by 4%. The change of PAOD with the DCM and hexane extractions is statistically insignificant because the population mean ratios overlap with that of the post-methanol extraction within one standard error. It appears that most of the effect of these two extraction stages has been to add noise; i.e., a widening of R_{tot} range rather than a shift in R_{tot}. The final NaOH extraction reduces the PAOD a further 9%, to 87% of the original PAOD on average; this change is statistically significant.

Therefore, we conclude that the fraction of visible light absorption due to water-insoluble OC can be largely attributed to NaOH-soluble HULIS, with a small fraction due to methanol-soluble OC. The water-insoluble but methanol-soluble OC are likely from biomass burning [*Chen and Bond*, 2010]. The water and methanol-insoluble, but NaOH-soluble, HULIS are likely humic acid that mostly comes from soil [*Graber and Rudich*, 2006]. No non-polar OC contribute to the light absorption, as hexane and DCM extractions do not reduce the total PAOD of LAP [*Polidori et al.*, 2008]. Since such non-polar OC is largely associated with direct emissions from anthropogenic sources (e.g., fossil fuel combustion), this lack of light absorption suggests a negligible contribution to visible light absorption due to OC from this source. Secondary production of particulate OC from such anthropogenic emissions would likely be polar and included in the methanol fraction.

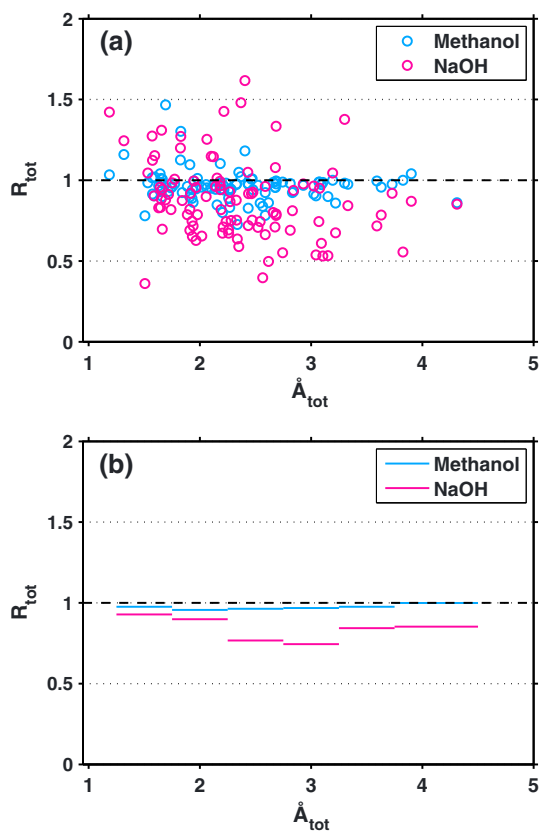

Figure 6. Ratio of R_{tot} after methanol and NaOH extractions versus $Å_{tot}$. $Å_{tot}$ is the average of the paired nuclepore samples quantified by optical measurement. Bars in part b show bin-median ratios in $\Delta Å_{tot} = 0.5$ intervals from $Å_{tot} = 1.25$ to $Å_{tot} = 4.25$.

As discussed in section 2.2, the fraction of absorption due to non-BC LAPs is related to the value of $Å_{tot}$, with higher values of $Å_{tot}$ corresponding to larger non-BC fractions of absorption. Therefore, we would expect the largest changes in R_{tot} to be associated with samples with higher values of $Å_{tot}$. Figure 6 shows the change in the ratio R_{tot} as a function of $Å_{tot}$ from the paired, unextracted nuclepore LAP samples. Because DCM and hexane do not significantly reduce the total optical depth of GHP samples, to avoid clutter, the data shown here are only for the methanol and NaOH extractions. Similar to what was shown in Figure 5, after methanol and NaOH extractions, the PAOD of most samples decreases while that of some samples increases (Figure 6a). Starting at $Å_{tot} = 1.25$, the median ratio R_{LAP} within intervals of $\Delta Å_{tot} = 0.5$ is shown in Figure 6b. From this we can see that the methanol extraction decreases the PAOD of samples approximately equally across the range of $Å_{tot}$. After NaOH extraction, which is the final stage of chemical extraction, R_{tot} decreases for all $Å_{tot}$ bins.

©2014. American Geophysical Union. All Rights Reserved.

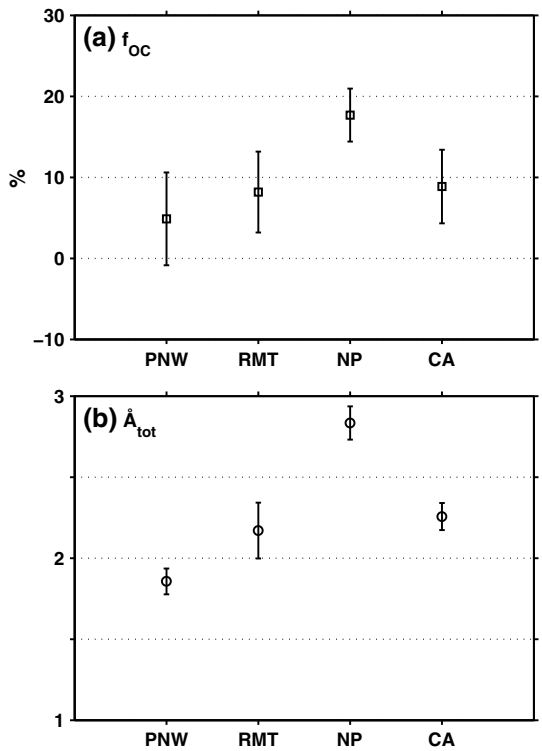

Figure 7. (a) Regional averages of the fractional light absorption (470–700 nm) due to total organic carbon (OC) (f_{OC}) extracted by all chemical solvents. (b) Regional averages of the absorption Ångström exponent, $Å_{tot}$, of the corresponding nuclepore samples. Error bars show standard error. Regions are PNW (Pacific Northwest), RMT (Rocky Mountains), NP (Northern Plains), and CA (Canada), per Figure 1.

The PAOD of samples with $Å_{tot}$ >2.25 are reduced the most significantly such that R_{tot} is as low as 0.75. By definition, as $Å_{tot}$ increases, the spectrally integrated PAOD of the particles is driven more by absorption at shorter wavelengths; i.e., a larger fraction of the absorption is likely due to OC, including HULIS. This is consistent with the PAOD of higher $Å_{tot}$ samples being reduced by a larger fraction after serial chemical extractions.

In order to examine regional differences in the PAOD partitioning, the regional mean fraction of the PAOD due to extractable OC is shown in Figure 7a. The sites that have available OC data are shown as red and blue markers in Figure 1. The mean fractional light absorption due to extractable OC in the Northern Plains is about 18%. This is about twice that of the Rocky Mountains (8%) and Canada (9%). The fractional absorption due to extractable OC is much lower in the Pacific Northwest, ~ 3%. Figure 7b shows that variations in regionally averaged $Å_{tot}$ parallel that of the extractable OC absorption in Figure 7a. This indicates that the results of the serial chemical extraction are consistent with the regional differences in the attribution of absorption to BC and non-BC constituents inferred from the ISSW measurements. The OC in the Northern Plains is different from the rest of the sampling regions, characterized by either a higher concentration of non-BC LAP or more-absorbing non-BC components. No statistically significant differences are found among the other three regions regarding fractional absorption due to extractable OC.

3.2. Comparison of Fractions of PAOD Attributed to non-BC

As discussed in section 2, the fraction of absorption due to non-BC LAPs can be estimated using the ISSW measurements alone, and this is done in standard ISSW analyses [e.g., *Doherty et al.*, 2010; *Wang et al.*, 2013]. Here we have presented an independent estimate of the fraction of absorption due to OC using serial chemical extractions. ICP-MS analyses of snow water samples can additionally be used to estimate the concentration of iron, and therefore absorption by iron oxides. Assuming all non-BC absorption in snow is due to organics and iron oxide, in Figure 8 we compare the fractional absorption due to all non-BC constituents derived solely from the optical (ISSW) analysis (f_{nonBC}) to the sum of OC and iron oxide absorption from the serial extractions (f_{OC}) and chemical analyses (f_{Fe}) discussed here. The sites for which both OC and iron were analyzed are shown as red markers in Figure 1. Note that the large error bars in both comparisons shown in Figure 8 are partly due to the limited number of samples that have both OC and iron data.

In all sampling regions, f_{nonBC} is generally higher than f_{OC} (green open circles in Figure 8). In the Northern Plains, f_{nonBC} is higher than f_{OC} by a factor of 2. For the other regions, f_{nonBC} is much higher than f_{OC}, especially in the Pacific Northwest, where the f_{OC} ~ 0 while the f_{nonBC} ~ 0.16. This strongly indicates that in all sampling regions, OC is not the only non-BC LAP in the snow.

Chemically derived fractions of PAOD due to all non-BC are calculated by adding f_{Fe} to f_{OC}. After including iron oxides, the non-BC fractional PAOD derived from the chemical methods increases substantially in all four regions (purple open squares). Comparing $f_{Fe} + f_{OC}$ with f_{nonBC}, we see that f_{nonBC} is higher by ~ 0.1 for all four regions.

©2014. American Geophysical Union. All Rights Reserved.

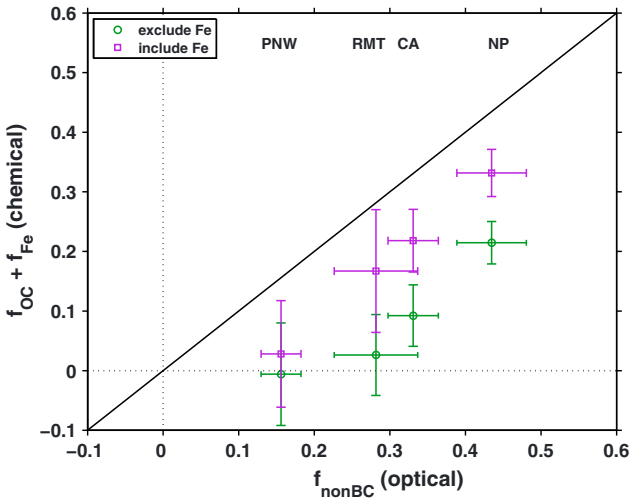

Figure 8. Comparison of non-black carbon (BC) fractional particulate light absorption optical depth (PAOD) (integrated from 470 to 700 nm) derived from two independent methods: chemical extraction (f_{OC}) + ICP-MS (f_{Fe}) and optical/ISSW analysis (f_{nonBC}). Regional means and one standard error are shown in the figure.

This indicates that either the optical method overestimates the absorption due to non-BC, or the chemical methods underestimate the absorption due to iron oxides and OC, or both.

In the optical analysis, the most obvious possible bias in partitioning absorption due to BC and non-BC (i.e., f_{nonBC}) lies in the assumptions we made for $Å_{nonBC}$ and $Å_{BC}$. We calculated $Å_{nonBC}$ based on measured soil $Å_{OC}$, assumed non-soil $Å_{OC} = 5$, and estimated the relative contributions of soil and other absorbers to non-BC absorption using receptor modeling. Therefore, the bias or uncertainty may first result from the inaccurate estimated relative contributions of soil and non-soil OC to non-BC absorption, which is impossible to quantify with the available data. Second, non-soil $Å_{OC}$ for these particles could be larger or smaller than 5. Referring to equation (2), when $Å_{tot}$ and $Å_{BC}$ are held constant, larger (smaller) $Å_{nonBC}$ will yield a smaller (larger) fraction of absorption optical depth attributed to non-BC. Similarly, if $Å_{tot}$ and $Å_{nonBC}$ are held constant, larger (smaller) $Å_{BC}$ will result in a smaller (larger) fractional absorption being attributed to non-BC, which can be easily illustrated by transforming equation (2) into $r_{nonBC} = 1 - \frac{Å_{nonBC} - Å_{tot}}{Å_{nonBC} - Å_{BC}}$. In addition, the assumed value of $Å_{BC}$ influences the spectral PAOD of BC, which is calculated by extrapolating the PAOD of BC at 525 nm to 470–700 nm using $Å_{BC}$, thus influencing the spectrally integrated value of f_{nonBC}.

For the chemical analysis, any bias most likely comes from calculating the fractional absorption due to iron oxides. To convert the iron oxide concentrations into PAOD, we estimated the MAC of iron to be 0.8 m^2/g at 550 nm. However, the actual MAC of ambient iron could be higher or lower than 0.8 m^2/g, resulting in a higher or lower fractional absorption attributed to iron. To extrapolate the PAOD of iron to 470 to 700 nm, we assumed that $Å_{Fe} = 3$, but $Å_{Fe}$ can vary from 3 to 6 [*Sherman and Waite*, 1985; *Marusak et al.*, 1980]. The estimated fractional absorption due to extractable OC, on the other hand, is less likely to produce bias in all sampling regions. This is because the chemical extraction introduces random noise, not systematic bias (as shown in Figure 5). However, if certain types of absorbing OC exist and are not dissolved in any of the four chemical solvents we selected, the estimated fractional absorption due to extractable OC could be biased low.

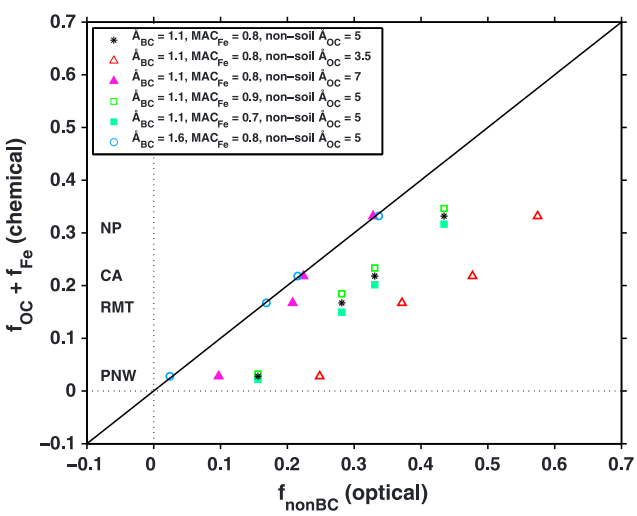

Figure 9. Comparison of non-BC fractional PAOD (integrated from 470 to 700 nm) derived from different methods with different conditions denoted in the legend. The black asterisk shows results of chemical and optical experiments. Others show results of sensitivity studies (see text).

To investigate the impact of the above possible biases, we did tests as shown in Figure 9. The values of $f_{Fe} + f_{OC}$ and

©2014. American Geophysical Union. All Rights Reserved.

f_{nonBC} denoted by black asterisks are the same as the purple open squares in Figure 3.4; we will call this the "base case" in the following discussion, for clarity. First, holding constant $Å_{BC}$ and the MAC of Fe, we replaced the non-soil $Å_{OC}$ with 3.5 and 7 following the uncertainty study by *Doherty et al*. [2010]. We then re-calculated f_{nonBC} using the optical measurements (triangles). When non-soil $Å_{OC}$ is 3.5, f_{nonBC} is much larger than in the base case, and when non-soil $Å_{OC}$ is 7, f_{nonBC} decreases and agrees much better with $f_{Fe} + f_{OC}$. Second, holding all other parameters fixed, we replaced the MAC of Fe with 0.9 and 0.7 [*Alfaro et al*., 2004] and then calculated the f_{Fe} from the chemical analysis (squares). When the MAC of Fe is larger (smaller), the f_{Fe} is larger (smaller) than that of the base case. Third, holding all other parameters constant, we changed $Å_{BC}$ until the difference between $f_{Fe} + f_{OC}$ and f_{nonBC} was minimized across the four regional averages. The resulting $Å_{BC}$ is equal to 1.6. According to the study of *Lack and Cappa* [2010], this is the theoretical upper limit possible for $Å_{BC}$. Besides these three cases, holding all other parameters constant, we also changed $Å_{Fe}$ to 6 and calculated f_{Fe}. The results show that f_{Fe} is approximately the same no matter if $Å_{Fe} = 3$ or $Å_{Fe} = 6$, so these results are not shown in Figure 9.

From the tests we can see that if we allow non-soil $Å_{OC}$, $Å_{BC}$ and MAC of Fe to each vary within their physically realistic range of values, (1) the change of non-soil $Å_{OC}$ produced the largest perturbation to f_{nonBC} and (2) the changes of MAC of Fe varied $f_{Fe} + f_{OC}$ slightly. When non-soil $Å_{OC}$ is equal to 7, the fraction of absorption due to non-BC estimated from chemical methods and optical methods is in agreement in the Northern Plains and Canada, and not terribly biased anywhere. For these fractions to be in agreement by instead altering $Å_{BC}$, the value of $Å_{BC}$ (i.e., 1.6) must be at the upper end of its physically possible range. For the chemically derived quantities, our estimate of f_{Fe} is not very sensitive to a realistic range of MACs for iron oxides. Therefore, we suspect that the underestimation of non-soil $Å_{OC}$ is responsible for most of the bias shown in Figure 3.4. Underestimation of $Å_{BC}$ and the MAC of Fe could be responsible for part of the difference, but they are unlikely the dominant component. Other factors, such as the change in the estimated relative contribution of non-soil OC and soil OC to light absorption, can influence f_{nonBC} but cannot be quantified in this experiment.

4. Discussion and Conclusions

In this paper, we applied chemical extraction to LAP samples collected in North America and on this basis partitioned the light absorption due to various types of OC. We then compared chemical and optical methods in estimating non-BC absorption.

Removal of methanol-soluble OC and NaOH-soluble HULIS reduces the absorption optical depth (PAOD, 470–700 nm) on the filters by 4 ± 1% and 9 ± 2%, respectively, while no significant reduction in PAOD is observed after DCM and hexane extractions. The fraction of absorption due to organics, f_{OC}, derived in this way is based on the measured PAOD of samples with and without extractable OC, with no assumptions regarding the species constituting the OC and their individual mass absorption coefficients needed. The methanol-soluble OC probably came from biomass burning, and the NaOH-soluble HULIS are humic acids, likely originating from soil or, possibly biomass burning. The ratio of absorption from soil based OC to that from biomass burning OC is thus 2.3. It is noteworthy that this value does not significantly differ from the ratio of soil absorption to combustion absorption derived from the PMF model (2.1) and used in the derivation of values for $Å_{nonBC}$ in section 2.2.

The contribution of iron oxides to the particulate absorption was also estimated based on analysis for iron in snow samples using ICP-MS; the values range from 3% to 70%, with a mean of 14%.

An independent optical method (ISSW) measures total absorption then separates BC and non-BC absorption based on the spectral dependence of their absorption. The resulting estimates of the fraction of non-BC absorption range from 20% to 80%.

The fraction of PAOD due to non-BC has thus been estimated in two independent ways: by chemical analyses and extractions, and by measurement of the filter's absorption spectrum alone. The chemically estimated fractional PAOD due to OC plus iron oxides is lower than the optically derived fractional PAOD due to non-BC and is subject to larger uncertainty in two of the four sampling regions, partly because the available iron data are limited. We show that non-BC fractional absorption estimated by the ISSW is perturbed most by changing the assumed value of non-soil $Å_{OC}$ within its physically plausible values.

There are still significant uncertainties associated with both the optical and chemical analyses. When coupling chemical extraction with the ISSW spectrophotometer to estimate the light absorption due to

©2014. American Geophysical Union. All Rights Reserved.

various types of OC, there are uncertainties associated with the change of LAP size distribution and mixture state, and the change of filter properties during chemical extractions. This results in a reduction of comparability in optical measurements before and after chemical extraction. For the optical methods, most of the uncertainty is associated with the assumption made for absorption Ångström exponents.

To improve the optical method, more accurate absorption Ångström exponents of non-BC LAPs in particular are needed. We expect that iron oxides and organic absorbers in soil and dust and organics in combustion aerosol ("brown carbon") are the main non-BC absorbers in snow, so measurements of absorption Ångström exponents for ambient OC and iron oxides are needed. For the chemical extraction procedure, the proper choice of filters and chemical solvents is crucial. Historically, chemical extraction experiments have been applied to lab-generated aerosols and airborne particulate samples. This study is, to our knowledge, the first such analysis done on LAPs collected from snow.

Acknowledgments
The LAP and snowmelt samples were collected in collaboration with Sarah Doherty, Stephen Warren, and Rudong Zhang. We thank Ariana Samuelson for working with us on the chemical extraction experiments during the summer of 2013. We thank Becky Alexander for providing some of the laboratory equipment. We thank Sarah Doherty, Stephen Warren, and Qiang Fu for helpful discussions. This research was supported by EPA STAR grant RD-82503801. This publication is funded by the Joint Institute for the Study of the Atmosphere and Ocean (JISAO) under NOAA Cooperative Agreement No. NA10OAR4320148, Contribution No. 2359. The data are available at http://www.atmos.washington.edu/Dang_and_Hegg_2014_data/. We also wish to acknowledge comments by two anonymous reviewers that have led to material improvement in the paper.

References

Alfaro, S. C., S. Lafon, J. L. Rajot, P. Formenti, A. Gaudichet, and M. Maillé (2004), Iron oxides and light absorption by pure desert dust: An experimental study, *J. Geophys. Res.*, *109*, D08208, doi:10.1029/2003JD004374.

Beine, H., C. Anastasio, G. Esposito, K. Patten, E. Wilkening, F. Domine, D. Voisin, M. Barret, S. Houdier, and S. Hall (2011), Soluble, light-absorbing species in snow at Barrow, Alaska, *J. Geophys. Res.*, *116*, D00R05, doi:10.1029/2011JD016181.

Bond, T. C. (2001), Spectral dependence of visible light absorption by carbonaceous particles emitted from coal combustion, *Geophys. Res. Lett.*, *28*(21), 4075–4078, doi:10.1029/2001GL013652.

Bond, T. C., et al. (2013), Bounding the role of black carbon in the climate system: A scientific assessment, *J. Geophys. Res. Atmos.*, *118*, 5380–5552, doi:10.1002/jgrd.50171.

Chen, Y., and T. C. Bond (2010), Light absorption by organic carbon from wood combustion, *Atmos. Chem. Phys.*, *10*(4), 1773–1787.

Clark, A. D., and K. J. Noone (1985), Soot in the Arctic snowpack: A cause for perturbations in radiative transfer, *Atmos. Environ.*, *19*, 2045–2053.

Clarke, A. D., K. J. Noone, J. Heintzenberg, S. G. Warren, and D. S. Covert (1987), Aerosol light absorption measurement techniques: Analysis and intercomparisons, *Atmos. Environ.*, *21*, 1455–1465.

Doherty, S. J., S. G. Warren, T. C. Grenfell, A. D. Clarke, and R. E. Brandt (2010), Light-absorbing impurities in Arctic snow, *Atmos. Chem. Phys.*, *10*(23), 11,647–11,680.

Doherty, S. J., T. C. Grenfell, S. Forsström, D. L. Hegg, R. E. Brandt, and S. G. Warren (2013), Observed vertical redistribution of black carbon and other insoluble light-absorbing particles in melting snow, *J. Geophys. Res. Atmos.*, *118*, 5553–5569, doi:10.1002/jgrd.50235.

Graber, E. R., and Y. Rudich (2006), Atmospheric HULIS: How humic-like are they? A comprehensive and critical review, *Atmos. Chem. Phys.*, *6*(3), 729–753.

Grenfell, T. C., S. J. Doherty, A. D. Clarke, and S. G. Warren (2011), Light absorption from particulate impurities in snow and ice determined by spectrophotometric analysis of filters, *Appl. Opt.*, *50*(14), 2037–2048.

Havers, N., P. Burba, J. Lambert, and D. Klockow (1998), Spectroscopic characterization of humic-like substances in airborne particulate matter, *J. Atmos. Chem.*, *29*(1), 45–54.

Hegg, D. A., S. G. Warren, T. C. Grenfell, S. J. Doherty, and A. D. Clarke (2010), Sources of light-absorbing aerosol in arctic snow and their seasonal variation, *Atmos. Chem. Phys.*, *10*(22), 10,923–10,938.

Intergovernmental Panel on Climate Change (2013), *Climate Change 2013: The Physical Science Basis. Contribution of Working Group I to the Fifth Assessment Report of the Intergovernmental Panel on Climate Change*, edited by T. F. Stocker et al., pp. 1535, Cambridge Univ. Press, Cambridge, U. K., and New York.

Kim, K. W., S. S. Park, K. H. Lee, and Y. J. Kim (2013), Atmospheric light extinction reconstructed from the size-resolved aerosol composition using PIXE analysis, *J. Korean Phys. Soc.*, *62*(1), 186–192.

Kirchstetter, T. W., T. Novakov, and P. V. Hobbs (2004), Evidence that the spectral dependence of light absorption by aerosols is affected by organic carbon, *J. Geophys. Res.*, *109*, D21208, doi:10.1029/2004JD004999.

Lack, D. A., and C. D. Cappa (2010), Impact of brown and clear carbon on light absorption enhancement, single scatter albedo and absorption wavelength dependence of black carbon, *Atmos. Chem. Phys.*, *10*(9), 4207–4220.

Lafon, S., J. L. Rajot, S. C. Alfaro, and A. Gaudichet (2004), Quantification of iron oxides in desert aerosol, *Atmos. Environ.*, *38*(8), 1211–1218.

Lafon, S., I. N. Sokolik, J. L. Rajot, S. Caquineau, and A. Gaudichet (2006), Characterization of iron oxides in mineral dust aerosols: Implications for light absorption, *J. Geophys. Res.*, *111*, D21207, doi: 10.1029/2005JD007016.

Marusak, L. A., R. Messier, and W. B. White (1980), Optical absorption spectrum of hematite, αFe_2O_3 near IR to UV, *J. Phys. Chem. Solids*, *41*(9), 981–984.

Pitchford, M., W. Malm, B. Schichtel, N. Kumar, D. Lowenthal, and J. Hand (2007), Revised algorithm for estimating light extinction from IMPROVE particle speciation data, *J. Air Waste Manage.*, *57*(11), 1326–1336.

Polidori, A., B. J. Turpin, C. I. Davidson, L. A. Rodenburg, and F. Maimone (2008), Organic PM 2.5: Fractionation by polarity, FTIR spectroscopy, and OM/OC ratio for the Pittsburgh aerosol, *Aerosol Sci. Technol.*, *42*(3), 233–246.

Sherman, D. M., and T. D. Waite (1985), Electronic spectra of Fe (super 3+) oxides and oxide hydroxides in the near IR to near UV, *Am. Mineral.*, *70*(11–12), 1262–1269.

Wang, X., S. J. Doherty, and J. Huang (2013), Black carbon and other light-absorbing impurities in snow across Northern China, *J. Geophys. Res. Atmos.*, *118*, 1471–1492, doi:10.1029/2012JD018291.

White, W. (1990), Contributions to light extinction, Chapter 4 in Visibility: Existing and historical conditions- causes and effects, Report 24, National Acid Precipitation and Assessment Program, published by The National Acid Precipitation Assessment Program, 722 Jackson Place NW, Washington, D. C.

Yang, L., X. Zhou, Z. Wang, Y. Zhou, S. Cheng, P. Xu, X. Gao, W. Nie, X. Wang, and W. Wang (2012), Airborne fine particulate pollution in Jinan, China: Concentrations, chemical compositions and influence on visibility impairment, *Atmos. Environ.*, *55*, 506–514.

Zhang, R., D. A. Hegg, J. Huang, and Q. Fu (2013), Source attribution of insoluble light-absorbing particles in seasonal snow across northern China, *Atmos. Chem. Phys.*, *13*(12), 6091–6099.

©2014. American Geophysical Union. All Rights Reserved.